SLAC – PUB – 3810
October 1985
T/E

Measurement of Elastic Electron Scattering from the Proton at High Momentum Transfer*

R. G. ARNOLD, P. E. BOSTED, C. C. CHANG†, J. GOMEZ,
A. T. KATRAMATOU, C. J. MARTOFF‡, G. G. PETRATOS,
A. A. RAHBAR, S. E. ROCK, A. F. SILL, Z. M. SZALATA

Department of Physics, The American University, Washington D.C. 20016

D. J. SHERDEN

Stanford Linear Accelerator Center, Stanford, CA 94305

J. M. LAMBERT

Department of Physics, Georgetown University, Washington D.C. 20057

R. M. LOMBARD-NELSEN

Dept. de Physique Nucleaire, CEN Saclay,
Gif-sur-Yvette, 91191 Cedex, France

Submitted to *Physical Review Letters*

* Work supported by U.S. Department of Energy contract DE-AC03-76F00515
† Permanent address: Department of Physics and Astronomy, University of Maryland, College Park, MD 20742
‡ Present address: Physics Department, Stanford University, Stanford, CA 94305

ABSTRACT

We have performed absolute measurements of the differential cross section for elastic e-p scattering in the range of momentum transfer from $Q^2 = 2.9$ to 31.3 $(\mathrm{GeV}/c)^2$. Combined statistical and systematic uncertainties in the cross section measurements ranged from 3% at low Q^2 to 19% at high Q^2. These data have been used to extract the proton magnetic form factor $G_M^P(Q^2)$. The results show a smooth decrease of $Q^4 G_M^P$ with momentum transfer above $Q^2 = 10$ $(\mathrm{GeV}/c)^2$. These results are compared with recent predictions of perturbative QCD.

We report new measurements of elastic electron scattering from protons which significantly increase the precision of the data at large values of four-momentum transfer squared (Q^2). The data are in agreement with previous measurements[1] at low Q^2 and extend to $Q^2 = 31.3$ $(\mathrm{GeV}/c)^2$. With some modest assumptions, these cross section measurements can be used to extract the proton magnetic form factor G_M^P with sufficient precision to allow a significant comparison with recent predictions of perturbative quantum chromodynamics (QCD).

The data reported here are from two experimental runs taken at the Stanford Linear Accelerator Center. The accelerator provided electrons with energies from $E = 5$ to 21.5 GeV in 1.6 μsec long pulses at up to 180 Hz, with typically 4×10^{11} electrons per pulse. The energy spread of the incident beam was limited by slits to typically $\pm 0.2\%$. The beam current was measured to within $\pm 0.5\%$ using two toroidal charge monitors.

Scattered electrons were detected in the SLAC 8 GeV/c spectrometer,[2] which was reassembled and outfitted with new detectors for this experiment. The spectrometer was positioned at angles of either $\theta = 21°$, 25°, or 33° to the beamline for most of the experiment. The detectors consisted of a sub-atmospheric nitrogen gas threshold Čerenkov counter, ten planes of proportional wire chambers, and a segmented lead glass shower counter. The Čerenkov counter and shower counter were used for electron identification and triggering. Together they provided a factor of 10^4 pion rejection while still retaining greater than 98% efficiency for detecting electrons. This reduced pion contamination of the elastic electron signal to a negligible level. The wire chambers were used to measure particle trajectories with a tracking efficiency of 98% to 99%.

Reconstruction of the particle trajectories allowed us to study the optics of the

spectrometer in detail. To check the effective dispersions for the horizontal and vertical scattering angles θ and ϕ, data were taken in the inelastic region using a tungsten grid to mask the entrance aperture of the spectrometer. The apparent spacings of holes in the grid were then compared with their physically surveyed values. The results agreed within errors and implied an overall uncertainty in acceptance of less than $\pm 2\%$.

Two liquid hydrogen targets of different lengths were used. The 25 cm target was used to determine the normalization of the acceptance for the 65 cm target, and for tests at low Q^2. The long target provided a higher counting rate than the short target and was used to take the majority of the elastic data. Two tungsten shields prevented particles which scattered from the endcaps of the long target from entering the spectrometer.

During the first part of the experiment, local beam-induced density changes were observed in the long target that gave corrections to the cross sections of $(5 \pm 2)\%$. Approximately 40% of the data at $Q^2 = 31.3$ $(\mathrm{GeV}/c)^2$ were taken under these conditions. During the second part of the experiment, improvements in the hydrogen flow reduced local density changes to an unmeasurable level. The resulting systematic uncertainty in target density is $\pm 1.0\%$ for the combined $Q^2 = 31.3$ $(\mathrm{GeV}/c)^2$ data sets, and $\pm 0.5\%$ for all other data.

At each of the spectrometer angle settings, the acceptance for each target was studied using deep inelastic electron scattering in kinematic regions where the cross section is well known. Within its apertures, the acceptance of the spectrometer depends on the momentum E' and horizontal and vertical scattering angles θ and ϕ of the particles. A central "fiducial" region in (E', θ, ϕ) space was defined such that for the short target, all particles with coordinates within that

region passed inside all of the apertures of the spectrometer. The E' and θ variation of the acceptance outside the fiducial region was determined for each target by comparing the counting rate at each (E', θ) bin to the fiducial value, correcting for the variation of the inelastic cross section and other known effects. The normalization between long and short targets was determined by comparing corrected short and long target counting rates in the fiducial region. To check the acceptance normalization, elastic data were taken at $Q^2 = 5$ $(\mathrm{GeV}/c)^2$ with both targets under identical kinematic conditions. An average difference in elastic cross sections of $(0.5 \pm 1.0)\%$ was observed. We assign a systematic error of $\pm 1\%$ to the cross sections to cover uncertainties in relative acceptance normalization.

The elastic cross section for each measurement was obtained by summing all counts with missing mass squared $W^2 \equiv M_P^2 + 2M_P(E - E') - Q^2$ between 0.7 and 1.1 $(\mathrm{GeV}/c)^2$, and applying the corrections indicated above. Data taken with empty target cells were used to subtract the counting rate due to the short target endcaps and to verify that backgrounds from the long target walls and endcaps were negligible. Missing mass histograms for the data points at the highest and lowest values of Q^2 are shown in Figure 1. Counting rates in the kinematically forbidden region of W^2 below the cut value of 0.7 $(\mathrm{GeV}/c)^2$ were negligible. A correction was also applied to account for the variation of the cross section with θ across the acceptance of the spectrometer.

Elastic radiative corrections were applied to the data using the formula of Mo and Tsai.[3] The radiative correction was typically 45%. To check the dependence of these corrections on external radiators, elastic data were taken with the short target at $Q^2 = 5$ $(\mathrm{GeV}/c)^2$ both with and without an additional 2.3% radiator upstream of the target. The final corrected cross sections agreed to within

$(2.0 \pm 1.5)\%$. As a check on possible angle dependence of radiative corrections and other effects, measurements were also made at $Q^2 = 5$ $(\mathrm{GeV}/c)^2$ at each of the three scattering angles (21°, 25°, and 33°) used in the experiment. The results for $Q^4 G_M^P$ agreed to within $(1.0 \pm 1.0)\%$, implying an agreement in cross sections to within $(2.0 \pm 2.0)\%$. We assign a systematic uncertainty of $\pm 1\%$ to the cross sections due to uncertainties in radiative corrections.

Other systematic effects could be produced on the cross section measurements due to uncertainties in the incident energy ($\Delta\sigma/\sigma = \pm(0.2$ to $0.8)\%$), final energy (0.5%), scattering angle (0.5%), incident beam angle ((0.5 to 1.0)%), and detector efficiencies (1.0%). When combined in quadrature with those discussed above, these contributions produce total systematic uncertainties of approximately $\pm 3\%$.

The elastic cross section can be represented in terms of the proton magnetic and electric form factors $G_M^P(Q^2)$ and $G_E^P(Q^2)$ as

$$\frac{d\sigma}{d\Omega} = \left(\frac{d\sigma}{d\Omega}\right)_{NS} \left\{ \frac{G_E^2(Q^2) + \tau G_M^2(Q^2)}{1+\tau} + 2\tau G_M^2(Q^2) \tan^2(\theta/2) \right\}$$

where $\tau \equiv Q^2/(4M_P^2)$, M_P is the proton mass, and $(d\sigma/d\Omega)_{NS}$ is the pointlike non-structure cross section. The Sachs form factors G_E and G_M are related to the Dirac and Pauli form factors F_1 and F_2 by the expressions $G_M = F_1 + F_2$ and $G_E = F_1 - \tau F_2$. F_1 corresponds to the helicity conserving part of the cross section, while F_2 corresponds to the helicity flip part.

At low momentum transfers ($Q^2 \leq 3$ $(\mathrm{GeV}/c)^2$), G_E^P has been found to scale[4] with G_M^P such that $G_E^P(Q^2) \approx G_M^P(Q^2)/\mu_P$ where μ_P is the proton magnetic moment (2.7928...). G_E^P has not been measured at high Q^2. If form factor scaling continues, the contribution of G_M^P to the cross section dominates over that of G_E^P at high Q^2. The contribution of G_E^P to the cross section under this assumption

is typically a few percent above $Q^2 = 5$ $(\mathrm{GeV}/c)^2$, and so moderate deviations from form factor scaling would have little effect on the extracted value of G_M^P for most of our data. Table I gives our cross section results and values of the proton magnetic form factor G_M^P assuming form factor scaling.

The data in Table I can be used to extract either G_M^P or F_1^P. Naive dimensional counting[7] predicts a $1/Q^4$ falloff of F_1^P, which is the principal contribution to G_M^P. The results for G_M^P are plotted in Figure 2, scaled by Q^4/μ_P. The data agree with previous measurements at low Q^2, reaching a broad peak near $Q^2 = 8$ $(\mathrm{GeV}/c)^2$, then exhibit a significant decrease with increasing Q^2. A straight line fit to the data between $Q^2 = 12.0$ $(\mathrm{GeV}/c)^2$ and $Q^2 = 31.3$ $(\mathrm{GeV}/c)^2$ shows a slope of $(-4.1 \pm 0.8) \times 10^{-3}$ $(\mathrm{GeV}/c)^2$ in that range. The curves shown in Figure 2 are the perturbative QCD predictions of references 5 and 6 using $\Lambda_{QCD} = 100$ MeV.

This experiment was motivated in part by perturbative QCD predictions[5,8,9] for the asymptotic behavior of proton form factors. Brodsky and Lepage[5] were able to calculate the evolution of G_M^P with Q^2, but not its overall magnitude. In these calculations F_2^P was neglected, and the results apply equally well to either F_1^P or G_M^P. Subsequently, Isgur and Llewellyn-Smith[10] calculated the overall normalization for the perturbative contribution to proton and pion form factors using a symmetric nonrelativistic wavefunction and obtained results two orders of magnitude below experiment. The proton form factor calculated with a symmetric asymptotic wavefunction $\phi_N(x) = 120x_1x_2x_3$ was shown to be identically zero.

Recent advances in quantum chromodynamics have been based on the use of sum rules[11] to estimate the moments of the hadron wavefunctions, includ-

ing nonperturbative contributions. The proton wavefunction evaluated by this method appears to differ dramatically from the asymptotic form.[6,12] Once a wavefunction has been found which has the moments predicted by QCD sum rules, the usual perturbative hard scattering formalism can be used to calculate specific properties, such as the proton form factors.

Chernyak and Zhitnitsky[6] have proposed a wavefunction which satisfies the sum rules and in which about 65% of the momentum of the proton is carried by one of its valence up quarks, with spin directed along the proton spin axis. Using this wavefunction, they calculate values for G_M^P which have approximately the correct normalization, within an overall uncertainty of a factor of two. Gari and Stefanis[13] have proposed an alternative wavefunction which also satisfies the sum rules, in which the two up quarks share most of the proton momentum. This wavefunction was chosen to yield neutron form factors in agreement with experiment, and also produces values of G_M^P with approximately the correct normalization. Other recent QCD analyses[14,15] are consistent with the use of an asymmetric wavefunction such as these.

Once the normalization of G_M^P is determined, the basic prediction of perturbative QCD can be tested. This prediction is that the evolution of F_1^P (and therefore G_M^P) with Q^2 is given by the running of the strong coupling constant $\alpha_s(Q^2)$, as described in reference 5. At high momentum transfer, this implies that $Q^4 G_M^P$ should decrease with increasing Q^2. The rate of decrease is given by the magnitude of the scale parameter Λ_{QCD}. Our results are in agreement with these expectations, as shown in Figure 2. It is clear that further theoretical work to establish the exact normalization of G_M^P and to extend the calculations beyond leading order would be justified by the precision of our new data.

We wish to acknowledge the support of D. Brown, J. Mark, J. Nicol, B. Smith, R. Eisele, and the rest of the SLAC staff, and valuable discussions with S. Brodsky and C. R. Ji. This work was supported under U.S. Department of Energy contract DE-AC03-76SF00515 (SLAC), and National Science Foundation Grants PHY83-40337 and PHY85-10549 (American University). One of us (J.G.) was partially supported by CONICIT, Venezuela.

REFERENCES

1. M. D. Mestayer, SLAC-214, Ph. D. thesis, Stanford University (1978) (unpublished);
   W. B. Atwood, SLAC-185, Ph. D. thesis, Stanford University (1975) (unpublished); W. B. Atwood, in *Proc. Summer Institute on Particle Phys., Stanford, CA, 1975*, SLAC-191, edited by M. C. Zipf (1976);
   G. Hohler *et al.*, Nucl. Phys. **B114**, 505 (1976);
   F. Borokowski *et al.*, Nucl. Phys. **B93**, 461 (1975), Nucl. Phys. **A222**, 269 (1974), Z. Phys. **A275**, 29 (1975);
   P. N. Kirk *et al.*, Phys. Rev. D **8**, 63 (1973);
   D. H. Coward *et al.*, Phys. Rev. Lett **20**, 292 (1968) and references contained therein.
2. SLAC User's Handbook, section D.3; see also Kirk *et al.*, Ref. 1.
3. L. W. Mo and Y. S. Tsai, Rev. Mod. Phys. **41**, 205 (1969)
4. T. Janssens *et al.*, Phys. Rev. **142**, 922 (1966);
   J. Litt *et al.*, Phys. Lett. **31B**, 40 (1970)
5. S. J. Brodsky and G. P. Lepage, Phys. Scripta **23**, 945 (1981);
   G. P. Lepage and S. J. Brodsky, Phys. Rev. D **22**, 2157 (1980);

G. P. Lepage and S. J. Brodsky, Phys. Rev. Lett. **43**, 545 (1979); ERRATUM-ibid. **43**, 1625 (1979)

6. V. L. Chernyak and I. R. Zhitnitsky, Nucl. Phys. **B246**, 52 (1984); V. L. Chernyak and A. R. Zhitnitsky, Phys. Rep. **112**, 173 (1984)
7. S. J. Brodsky and G. Farrar, Phys. Rev. **D11**, 1309 (1975); S. J. Brodsky and B. T. Chertok, Phys. Rev. **D14**, 3003 (1976)
8. A. Duncan and A. H. Mueller, Phys. Lett. **90B**, 159 (1980); A. Duncan and A. H. Mueller, Phys. Rev. D **21**, 1636 (1980)
9. R. Coquereaux and E. de Rafael, Phys. Lett. **74B**, 105 (1978)
10. N. Isgur and C. Llewellyn-Smith, Phys. Rev. Lett. **52**, 1080 (1984)
11. M. A. Shifman, A. I. Vainshtein and V. I. Zakharov, Nucl. Phys. **B147**, 385 (1979). Sum rules have since been investigated by many authors.
12. Some of the sum rule predictions for the moments for the proton wavefunction given in reference 6 have been separately obtained by M. J. Lavelle, Nucl. Phys. **B260**, 323 (1985)
13. M. Gari and N. G. Stefanis, preprint RUB-TP11-85-16, December 1985 (unpublished).
14. A. Andrikopolou, J. Phys. **G11**, 21 (1985)
15. C. E. Carlson, Lectures given at the NATO Advanced Study Inst., Banff, Canada, Aug 22 - Sep 4, 1985

Table 1. Cross Sections and Extracted Values of G_M^P Assuming $G_E^P = G_M^P/\mu_P$						
E GeV	E' GeV	θ deg	Q^2 $(\mathrm{GeV}/c)^2$	$d\sigma/d\Omega \pm$ stat $\pm$ syst nanobarns/steradian	Portion of σ due to G_M^P	$Q^4 G_M^P/\mu_P \pm$ stat $\pm$ syst $(\mathrm{GeV}/c)^4$
5.483	3.953	21.01	2.883	$0.796 \pm 0.009 \pm 0.026$	87.8%	$0.336 \pm 0.002 \pm 0.006$
5.483	3.546	25.01	3.646	$0.190 \pm 0.004 \pm 0.006$	90.6%	$0.363 \pm 0.004 \pm 0.006$
7.640	4.950	21.01	5.028	$(6.91 \pm 0.03 \pm 0.22) \times 10^{-2}$	92.9%	$0.387 \pm 0.001 \pm 0.006$
6.676	4.000	25.01	5.008	$(4.53 \pm 0.08 \pm 0.14) \times 10^{-2}$	93.2%	$0.393 \pm 0.003 \pm 0.006$
5.507	2.830	33.01	5.032	$(2.03 \pm 0.03 \pm 0.07) \times 10^{-2}$	94.1%	$0.387 \pm 0.003 \pm 0.006$
9.625	5.730	21.01	7.334	$(1.08 \pm 0.02 \pm 0.04) \times 10^{-2}$	95.2%	$0.401 \pm 0.004 \pm 0.007$
11.47	6.330	21.01	9.656	$(2.54 \pm 0.06 \pm 0.08) \times 10^{-3}$	96.4%	$0.395 \pm 0.005 \pm 0.007$
13.22	6.830	21.01	12.01	$(8.01 \pm 0.22 \pm 0.26) \times 10^{-4}$	97.2%	$0.392 \pm 0.005 \pm 0.006$
15.86	7.478	21.01	15.77	$(1.73 \pm 0.09 \pm 0.06) \times 10^{-4}$	98.0%	$0.375 \pm 0.009 \pm 0.006$
18.38	7.993	21.01	19.53	$(4.72 \pm 0.32 \pm 0.16) \times 10^{-5}$	98.4%	$0.348 \pm 0.012 \pm 0.006$
20.81	8.422	21.01	23.31	$(1.85 \pm 0.15 \pm 0.06) \times 10^{-5}$	98.7%	$0.351 \pm 0.014 \pm 0.006$
21.20	6.810	25.01	27.08	$(4.05 \pm 0.50 \pm 0.13) \times 10^{-6}$	99.1%	$0.324 \pm 0.019 \pm 0.005$
21.20	4.570	33.01	31.28	$(8.2 \pm 1.5 \pm 0.3) \times 10^{-7}$	99.5%	$0.339 \pm 0.031 \pm 0.006$

FIGURE CAPTIONS

1. Histograms of counts vs. missing mass squared at the highest and lowest values of Q^2 in this experiment. (a) $Q^2 = 2.883$ $(\mathrm{GeV}/c)^2$. (b) $Q^2 = 31.28$ $(\mathrm{GeV}/c)^2$. The curves show the expected resolution of the apparatus for each case as determined from a Monte Carlo simulation of the experiment, including acceptance and radiative effects, but neglecting inelastic reactions.

2. Extracted Values of $Q^4 G_M^P/\mu_P$ vs. Q^2. Open circles show previous data as given in reference 1. Solid circles show the results of this experiment. The curves show the perturbative QCD predictions of references 5 (BL) and 6 (CZ) for $\Lambda_{QCD} = 100$ MeV.

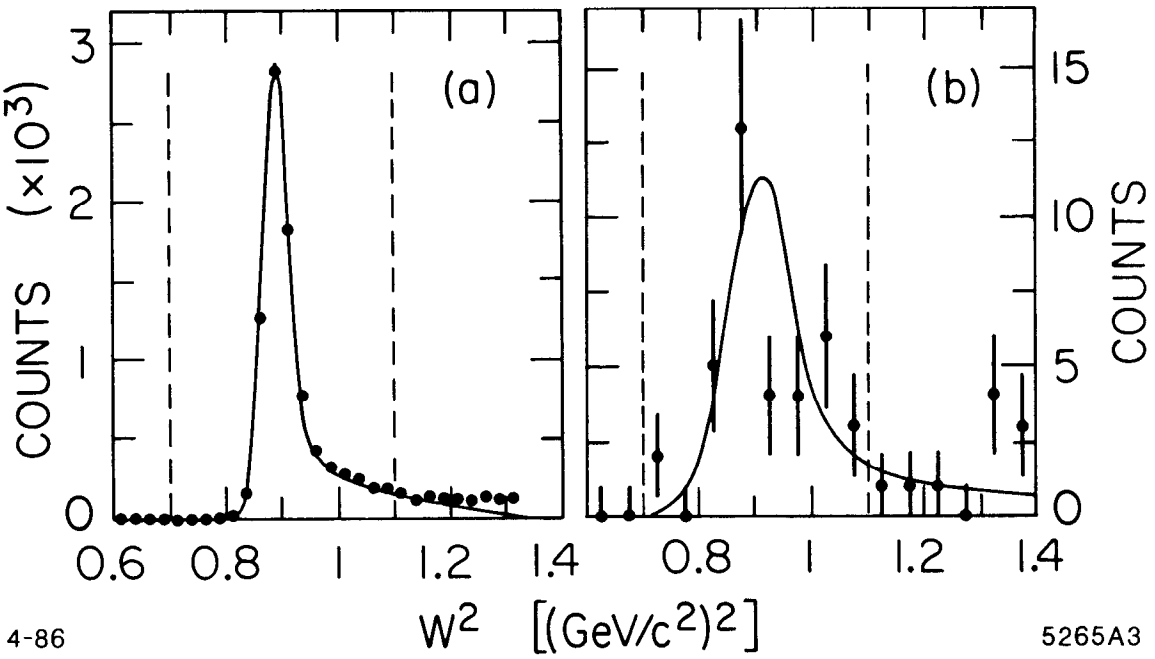
COUNTS (×10³)
3
2
1
0
(a)
(b)
15
10
5
0
COUNTS
0.6
0.8
1
1.2
1.4
0.8
1
1.2
1.4
W² [(GeV/c²)²]
4-86
5265A3

Fig. 1

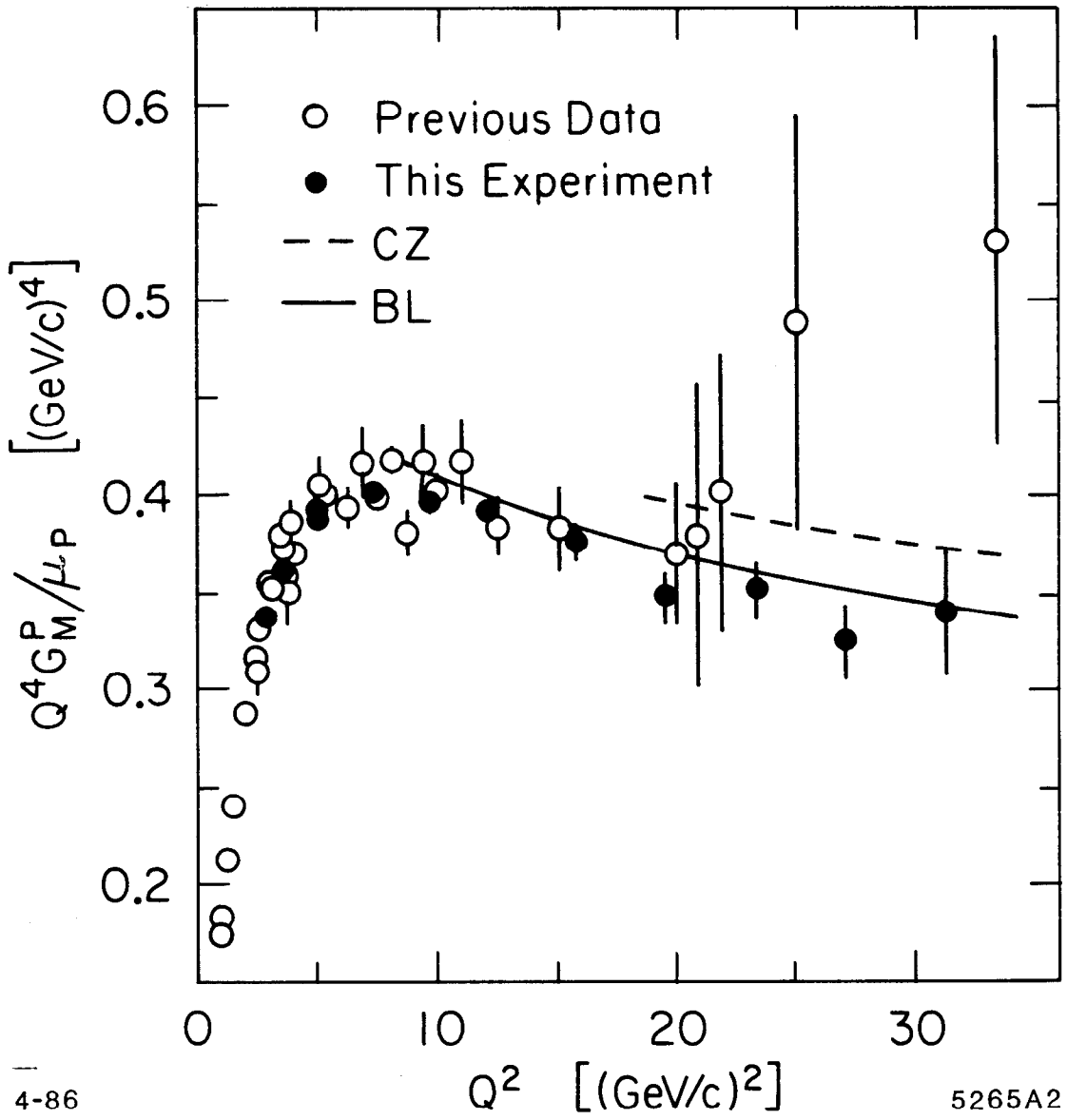
Previous Data
This Experiment
CZ
BL
0.6
0.5
0.4
0.3
0.2
0
10
20
30
$Q^4G_M^P/\mu_P$ [(GeV/c)^4]
Q^2 [(GeV/c)^2]
4-86
5265A2

Fig. 2